Microfluidic guillotine for single-cell wound repair studies

Lucas R. Blauch[a], Ya Gai[a], Jian Wei Khor[a], Pranidhi Sood[b], Wallace F. Marshall[b], and Sindy K. Y. Tang[a,1]

[a]Department of Mechanical Engineering, Stanford University, Stanford, CA 94305; and [b]Department of Biochemistry and Biophysics, University of California, San Francisco, CA 94143

Edited by Jennifer Lippincott-Schwartz, Howard Hughes Medical Institute, Ashburn, VA, and approved June 6, 2017 (received for review March 28, 2017)

Wound repair is a key feature distinguishing living from nonliving matter. Single cells are increasingly recognized to be capable of healing wounds. The lack of reproducible, high-throughput wounding methods has hindered single-cell wound repair studies. This work describes a microfluidic guillotine for bisecting single *Stentor coeruleus* cells in a continuous-flow manner. *Stentor* is used as a model due to its robust repair capacity and the ability to perform gene knockdown in a high-throughput manner. Local cutting dynamics reveals two regimes under which cells are bisected, one at low viscous stress where cells are cut with small membrane ruptures and high viability and one at high viscous stress where cells are cut with extended membrane ruptures and decreased viability. A cutting throughput up to 64 cells per minute—more than 200 times faster than current methods—is achieved. The method allows the generation of more than 100 cells in a synchronized stage of their repair process. This capacity, combined with high-throughput gene knockdown in *Stentor*, enables time-course mechanistic studies impossible with current wounding methods.

microfluidics | single cell | wound healing | microguillotine | *Stentor coeruleus*

Wound repair is an essential biological process for maintaining homeostasis and, ultimately, for survival. Compared with tissue-level wound healing, how individual cells heal wounds and regenerate damaged or lost cellular structures is less understood (1). Nevertheless, there is increasing recognition that single cells—such as muscle cells and neurons—are capable of wound repair (1–3). Understanding how single cells repair themselves is critical for determining fundamental cellular functions, and eventually for revealing how wound-induced diseases such as muscular dystrophies develop.

Thus far, studies of single-cell wound response have been performed in a few model organisms (1, 4, 5). In particular, studies performed in *Xenopus* oocytes elegantly leveraged the unique advantages of the oocyte system, including the large size and the ability to create and visualize a wound in the focal plane of the microscope, to shed light on cellular components participating in wound healing and to reveal their dynamic interactions through live cell imaging. Nevertheless, as with any model system, *Xenopus* oocytes are better suited to some types of experiments than to others. For example, oocytes are transcriptionally inactive and are preloaded with large stockpiles of mRNA; they are thus not a good system for investigating transcriptional response to wounding. To interfere with protein production in *Xenopus* oocytes, morpholino oligonucleotides are injected to inhibit mRNA translation to prevent protein production (6). This method is expensive due to the high cost of synthesizing morpholino oligos. The need to inject cells one at a time also limits the throughput of the approach. In addition, because oocytes are loaded with maternally derived protein, protein depletion may be incomplete even when translation is entirely blocked. It is also a potential concern that the morpholino injection process inevitably wounds the cells. By the time one performs wound-healing assay the cells may have already undergone a wound-healing cycle and may therefore be in an unusually primed state. As such, there is a need for a complementary system to *Xenopus* oocytes that would be more amenable to high-throughput gene knockdown approaches and transcriptional profiling analysis. Ideally, such system should be compatible with simple and cost-effective methods for altering gene expression, such as RNAi by feeding, to facilitate the study of a large number of cells without wounding the cells during the gene alteration process.

Here, we use *Stentor coeruleus* as a model organism for single-cell wound repair studies because it satisfies such requirement (7–9). *Stentor* is a single-celled ciliate protozoan that is up to 1 mm long. They exist as single cells and are regularly wounded under physiological conditions (e.g., attacks by predators) (10) and are known to be capable of recovering robustly from drastic wounds and regenerating from cell fragments as small as 1/27th of the original cell size (11, 12). *Stentor* was a popular organism in the early 1900s (11) but was never developed as a molecular model system partly because culturing in large quantities was difficult. With the advent of low-input next-generation sequencing tools, it has become feasible to develop *Stentor* as a model organism. The genome of *Stentor* has recently been published (9). We have also demonstrated the utility of RNAi to knock down gene expression, by feeding *Stentor* bacteria containing an expression plasmid encoding dsRNA that targets genes of interest (7, 8). *Stentor* thus offers a substantial technical advantage over *Xenopus* oocytes for high-throughput knockdown studies.

To take full advantage of high-throughput gene knockdown, a method is required for wounding cells in a concomitantly high-throughput manner. Rapid, high-throughput wounding is also critical for ensuring sufficient time resolution in subsequent observations, because wound repair is intrinsically a dynamic process. In *Stentor*, regeneration is resolved into a series of morphological steps, each of which takes about 1 h (13). Any study that aims to

Significance

Whereas tissues can repair wounds regularly, single cells—including muscle cells, neurons, and cancer cells—are increasingly recognized to have a wound response. Ability to understand and control single-cell repair holds the potential for new strategies to treat human diseases. Existing wounding methods and model organisms are insufficient for elucidating the biological mechanisms involved. This paper reports a microfluidic guillotine for the high-throughput bisection of hundreds of cells reproducibly. The fine time resolution achieved enables mechanistic studies critical for a molecular understanding of single-cell wound repair currently impossible with existing wounding methods. The work here will lay the foundation for understanding how single cells heal themselves, a fundamental feature distinguishing living from nonliving matter.

Author contributions: L.R.B., W.F.M., and S.K.Y.T. designed research; L.R.B., Y.G., and J.W.K. performed research; P.S. contributed new reagents/analytic tools; L.R.B., Y.G., J.W.K., and S.K.Y.T. analyzed data; and L.R.B., Y.G., J.W.K., P.S., W.F.M., and S.K.Y.T. wrote the paper.

The authors declare no conflict of interest.

This article is a PNAS Direct Submission.

[1]To whom correspondence should be addressed. Email: sindy@stanford.edu.

This article contains supporting information online at www.pnas.org/lookup/suppl/doi:10.1073/pnas.1705059114/-/DCSupplemental.

ENGINEERING

probe the mechanism and time evolution of wound repair will require a method that can generate a large number of cells wounded on a time scale that is short compared with the time scale of repair, so that all cells are relatively synchronized in their stage of the process. Unfortunately, the traditional wounding method based on the manual manipulation of glass needles is too slow to meet this need (14, 15). It takes ∼3 min to wound one cell depending on the skill of the experimenter. Obtaining 100 cells would take 5 h, during which much healing and regeneration would have already occurred. Additionally, wounding groups of cells to the same degree is challenging, because controlling wound size with manual cutting is difficult. It is thus impossible to perform time-course experiments involving analysis such as RNA sequencing, which typically requires hundreds of cells.

An alternative method using laser ablation has been applied to introduce wounds in other cell types (16–19). Laser wounding is directly compatible with imaging-based analysis because it can be performed through the same microscope that is used for subsequent imaging. The throughput is relatively low, however, because the laser spot has to be repositioned and refocused to wound each new cell. The ideal wound-healing assay for our purposes should introduce wounds at a throughput much higher than that allowed by traditional manual dissection methods.

In this paper, we aim to solve the above limitations by using a microfluidic guillotine device to automate the cutting of *Stentor* cells in a continuous-flow manner. Instead of moving a sharp object (e.g., a knife) against a relatively immobile cell (20), we flow the cell into a knife with a fixed position inside a microfluidic channel. Our design has two key advantages: (*i*) The confinement of the cell in the microchannel allows simple positioning of a cell to the knife, and (*ii*) it facilitates the processing of a continuous stream of cells in a flow-through manner, because cut cells can be flushed out of the channel easily. In the first demonstration of principle, we focus on the bisection of cells. We monitor the shape of the cell during the cutting process at different applied flow conditions and measure the subsequent cell viability. We believe that our microfluidic platform will lay the foundation critical for using *Stentor* to understand how single cells heal wounds and regenerate.

Results and Discussion

Design and Validation of the Microfluidic Guillotine Device. Fig. 1*A* shows a scheme of the microfluidic guillotine device. The knife consisted of a simple triangular blade made in polydimethylsiloxane (PDMS). A cell injected into the microchannel was cut at the knife, and the two halves of the cut cell ("fragments") flowed into the two outlet channels. We found that the PDMS knife was sufficiently stiff and effective to cut *Stentor*, although PDMS is relatively soft (Young's modulus ∼500 kPa). In all our experiments we did not observe any deformation in PDMS itself. Although we have not measured the Young's modulus of *Stentor*, we expect its value to be close to that of unicellular *Dictyostelium* (∼1–8 kPa) (21), about 100 times smaller than that of PDMS. To facilitate the efficient cutting of *Stentor* we used channels with dimensions smaller than the size of a cell (Table S1). This confinement ensured the cells were cut at the knife and prevented them from bypassing the knife and flowing into one of the outlets without being cut. To ensure cells were cut into approximately equal halves we included fluidic shunts immediately downstream of the knife. The shunts helped to equalize the pressure in the two outlets and to avoid disturbance to the cutting process arising from changes in the fluidic resistance at the outlet (22, 23).

Fig. 1*B* shows images of the cell during the cutting process at a flow rate of Q = 0.36 mL/h. The cutting process involves three basic steps. (*i*) The cell comes into contact with the knife tip. (*ii*) The cell extends into the two branches downstream, but its rear end remains attached at the knife tip. (*iii*) As the cell continues to extend downstream, the rear end of the cell at the knife tip decreases in thickness and stretches into a thin thread, which eventually snaps off and the cell is split into two fragments that flow downstream separately.

To validate our microguillotine, Fig. 1*C* shows images of the regeneration of two cell fragments at different times after a single cell was cut by our device. Fig. 1*D* shows a similar set of images from a different cell cut manually using a glass needle. See Movies S1 and S2 for corresponding videos. Both cells cut by our device and by hand were able to survive and regenerate normal morphology within 24–48 h. The typical *Stentor* cell cycle length is 3 d (24), and we observed that cells cut with either method survived for at least 5 d, at which point they had often undergone cell division to form new cells. These observations show that the cells had recovered important features indicating viability.

Effect of Applied Viscous Stress on Cell Deformation and Survival. Fig. 2 shows the effect of the applied flow rate at a fixed blade angle of 6°. We have chosen to use this blade angle because we were able to obtain the highest cell survival rate at ∼97% compared with large blade angles (Fig. S1). Based on the cell extension length and survival data, we separated the flow into two regimes: regime I ($v \leq v_c$), and regime II ($v > v_c$), where v_c ∼1.5 cm/s.

In regime I, the viscous stress was low. The cells spanned the whole width of the channel before, during, and at the completion of the cut (Fig. 2*A* and Movies S3 and S4). The cell did not undergo large deformation. The maximum extension length was small, $\varepsilon_{max} \lesssim 2$ (Fig. 2*B*). In this paper, the extension lengths reported were normalized to the length of the major axis of the uncut cell before it contacted the knife (*Materials and Methods*). In addition, the cells always split at the knife tip into two cell fragments that were approximately equal in size. The difference in the size of the two fragments was, on average, 10–16% of the mean size of the two cell fragments. Although we were not always able to differentiate the membrane from the cell content using our imaging setup, the membrane seemed to rupture only at the knife tip at the end of the cutting process in most of the cuts. The cell content typically stayed inside the cell during the entire process. The cell survival rate was above 90% (Fig. 2*C*).

In regime II, the applied flow rate—and thus the viscous stress experienced by the cells—increased. We observed changes in the morphology of the cell distinct from that in regime I during the cutting process. Whereas the cells spanned the whole width of the channel before the cut, they became highly stretched during the cut and did not span the whole width of the channel before the cut completed (Fig. 2*A* and Movie S5). The membrane rupture was no longer confined to the rear end of the cell at the knife tip. The membrane often tore at multiple locations downstream of the knife and led to spilling of cell content. The extension length increased with velocity, reaching ε_{max} ∼3 (Fig. 2*B*). Because we could not easily identify the cell membrane, the increased extension length reported here was contributed by both an increase in membrane deformation and an increase in cell content spilled out. As velocity increased the cells also tended to split into two or more fragments at random locations downstream of the knife tip. The sizes of the fragments were, therefore, less uniform than those cut in regime I. The corresponding cell survival rate also decreased from close to 100% to ∼60% (Fig. 2*C*).

In our design there are two possible sources of stress that can act together to cut the cell. The first source arises from the cell pushed normal against the knife by the fluids. This stress could lead to a cutting mechanism where the knife tip penetrates the cell membrane, followed by the splitting of cell content into two halves. The second source is a viscous stress provided by the flow around the cell. This stress tends to lead to the tearing of the membrane. Depending on the detailed local hydrodynamics and mechanical properties of the cell, the rupture could occur at the tip of the blade or other parts of the cell.

In regime I, it was unlikely that the knife had penetrated the cell membrane upon initial contact. Instead, the cells were often

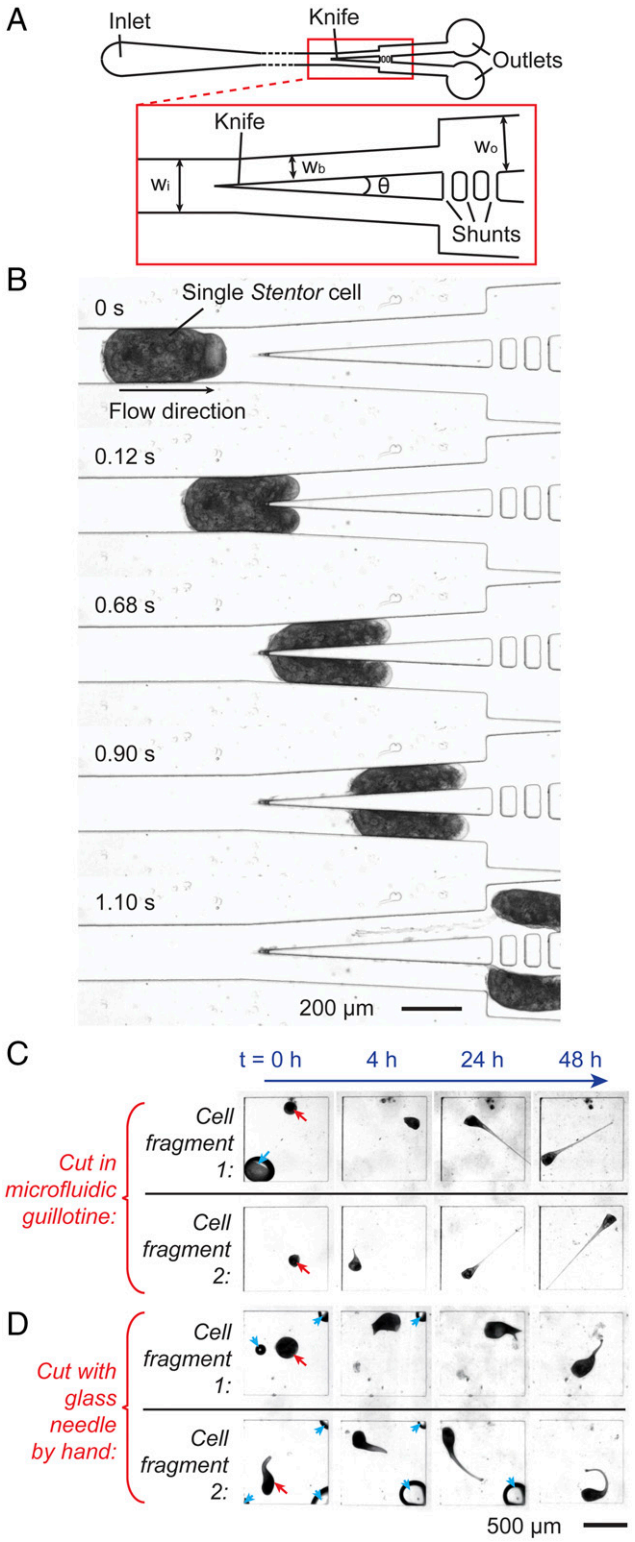

Fig. 1. Design and validation of the microfluidic guillotine device and regeneration of cell fragments. (*A*) Scheme of the microfluidic guillotine device. The red box shows details of the knife region. The dimensions are listed in Table S1. (*B*) Micrographs showing the time sequence of the flow of a *Stentor* cell in the microchannel, the bisection of the cell at the knife, and the subsequent splitting of the two cell fragments into two separate outlets downstream. (*C*) Micrographs of the regeneration process (at time t = 0, 4, 24, and 48 h after the cut) of two cell fragments generated from cutting one cell using the microfluidic guillotine. (*D*) Micrographs of the regeneration process (at time t = 0, 4, 24, and 48 h after the cut) of two cell fragments generated from cutting one cell using a glass needle by hand. The two fragments (indicated by red arrow at t = 0) were kept in two separate PDMS wells. By t = 24–48 h all cell fragments have regenerated their trumpet shapes. The blue arrows indicate air bubbles that dissolved eventually. Videos of regeneration for *A* and *B* are shown in Movies S1 and S2, respectively.

observed to wrap around the knife blade without being punctured initially. As the cell continued to flow downstream the membrane at its rear end stretched and eventually pinched off at the knife tip (Movie S4). The pinch-off was driven primarily by viscous stress close to the knife tip. The degree of membrane rupture seemed to be relatively small and confined to the rear end of the cell only (Fig. S2). In regime II, the pressure exerted on the cell by the knife at the flow rates applied could approach that needed to penetrate the membrane. It thus became possible that the knife had punctured the membrane as the cell first contacted the knife, although an improved imaging setup will be necessary to verify this process. Nevertheless, in this regime the high viscous stress experienced by the cell led to an increased extension of the cell and caused membrane ruptures at multiple locations downstream of the knife tip. The predominant way that cells were cut arose from these ruptures, which led to the splitting of the cell into fragments of different sizes along with extensive spilling of the cytoplasm.

Transition from Regime I to Regime II. The identification of the threshold velocity has immediate practical value in guiding the choice of channel geometry and experimental conditions. Because cell survival decreased rapidly in regime II, the maximum velocity to cut the cells to achieve a high throughput of cutting while maintaining cell viability is at the threshold velocity when regime I transitions to regime II.

To probe why the transition occurred at a velocity of $v_c \sim 1.5$ cm/s would require further characterization of the mechanical properties of *Stentor*. The properties of the cell membrane and cell content are highly nonlinear, anisotropic, and heterogeneous and are an active area of research (25, 26). Interestingly, we found that the morphology of the cell during the cut was similar to that of a shear-thinning viscoelastic drop, which also exhibited a transition from regime I to regime II when we increased the velocity of flow above a critical velocity (Fig. S3). Such similarity suggests that the critical velocity for the cutting of the cell in our device could perhaps be modeled without having to consider the entirety of the complex internal structure and rheology of the cell.

The Relationship Between Cell Deformation and Survival. Fig. 2 *B* and *C* show that, in general, cell extension or deformation was inversely related to survival rate. The increased spread of data in regime II reflects that the location where the cell split, the number and the size of the cell fragments, and the corresponding wound sizes were less controlled than that in regime I. The relationship between cell extension and survival here is qualitatively consistent with previous work that reported that large deformation increased the strain on the surface of the cell, and thus the likelihood of cell lysis and cell death (27, 28).

There are key differences between the cells studied previously (e.g., human prostate primary adenoma cancer cells and mouse myoblasts) and *Stentor*, however. For example, when the cell membrane expanded beyond ~50%, the viability of human prostate primary adenoma cancer cells was reported to decrease rapidly as evidenced by cell lysis (27). However, most of the *Stentor* cells survived in regime I even though their normalized extension length increased to $\varepsilon_{max} \sim 2$, corresponding to up to a doubling of its apparent surface area. This capability was in part due to the ability of *Stentor* to deform: We and others have observed that *Stentor* can contract to 20–25% of its extended length in milliseconds when

ENGINEERING

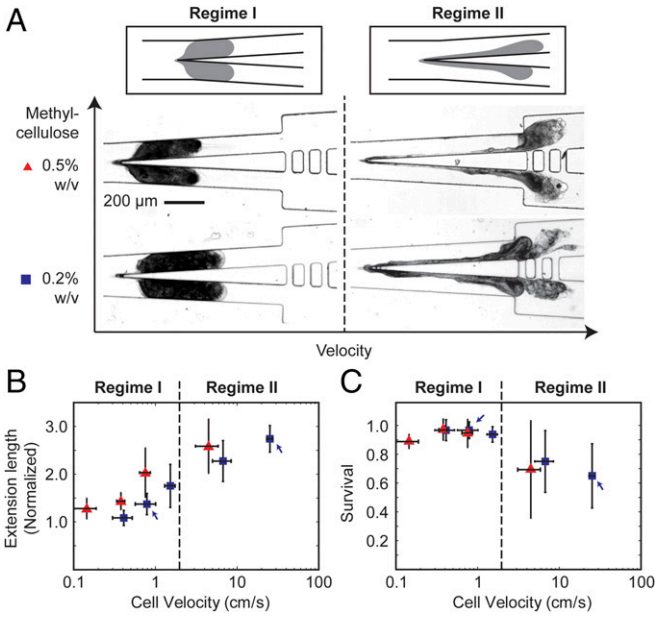

Fig. 2. Characterization of the effect of applied flow rate on the cutting process and cell survival. (*A*) Schemes and micrographs showing the morphology of the cell during the cutting process at low velocity (regime I) and high velocity (regime II). For each case, the cells were suspended in a methylcellulose solution at a concentration of 0.2% wt/vol or 0.5% wt/vol. (*B*) The normalized extension length of the cell during cutting and (*C*) cell survival rates, as a function of cell velocity measured immediately upstream of the knife. The blue and red symbols correspond to experiments performed in 0.2% and 0.5% methylcellulose solutions, respectively. In *B*, the markers indicate the mean from 7 cells. In *C*, the markers indicate the mean from four to seven cells from each of the three separate experiments (or total of >15 cells from all experiments). The height of the error bar represents one SD from the mean. The width of the error bar represents one SD from the mean cell velocity at a fixed flow rate as applied from the syringe pump.

stimulated mechanically (29–31). Left undisturbed, *Stentor* returns to its extended state in a few seconds. In addition, *Stentor* survived after being split into two fragments, during which the membrane must have opened (and the cell must, therefore, have been "lysed"). Indeed, *Stentor* have been observed to be capable of recouping the cytoplasm from membrane ruptures and surviving afterward (32), as well as surviving grafting experiments in which two cut cells were fused together at the site of the cuts (33, 34). These results, along with those presented in this paper, indicate that membrane rupture alone did not lead to immediate cell death in *Stentor*.

Nonetheless, cells undergoing large deformation in regime II also tended to have increased membrane ruptures that led to increased spillage of the cell content. We believe that the increased loss of cell content eventually led to decreased cell survival here. To probe the degree of membrane rupture, we used a small, negatively charged fluorophore, bis-(1,3-dibutylbarbituric acid)trimethine oxonol [DiBAC4(3)], which is typically membrane-impermeable (35, 36). It can enter depolarized cells and bind to intracellular proteins or membranes to exhibit increased fluorescence intensity.

Fig. 3 shows that when the cell was intact, DiBAC4(3) could not permeate the membrane and was barely fluorescent. When the cell was cut, its membrane ruptured. *Stentor*, having an approximate resting membrane potential of –50 mV, became depolarized (37). At the same time, the intracellular proteins became exposed to the media containing DiBAC4(3). The fluorescence intensity of DiBAC4(3) increased from that in intact cells.

In general, fluorescence intensity should increase with increasing wound size because more DiBAC4(3) could enter the cell and interact with intracellular proteins. Indeed, the fluorescence intensity of DiBAC4(3) in cells cut in regime I was not significantly different from that in uncut cells. In contrast, the fluorescence intensity in cells cut in regime II was, on average, 20 times higher than in uncut cells. The location of the fluorescence also correlated with the part of the cell where the membrane seemed to be missing (Fig. 3*A*). These observations confirm that the wound size was smaller when the cells were cut under low viscous stress than when they were cut under high viscous stress, in agreement with the measured cell extension and survival data in Fig. 2 *B* and *C*.

We note the spread of the fluorescence data were larger in cells cut in regime II than in cells cut in regime I. For example, there were cells that exhibited fluorescence up to six times higher than the mean in the same experiment. They corresponded to severely wounded cells with visibly disrupted membranes. These cells were unlikely to survive, partly supported by the fact that dead cell fragments, which have lost their membrane integrity, were even more fluorescent than the severely wounded cells. There were also cells that exhibited low fluorescence (<1,000 in absolute fluorescence intensity, Fig. 3*B*) similar to those of cells cut in regime I. These cells were likely to survive. We counted the number of cells that had low levels of fluorescence ($n = 20$) versus those that were highly fluorescent ($n = 11$), and the percentage of cells with low fluorescence was about 64%. This value corresponded well with the 60% survival rate in regime II (Fig. 2*C*).

Furthermore, we performed the same assay on the cut cells after 24 h. We first identified cells that were alive (*Materials and Methods*) and then measured the fluorescence of these cells. We found that all cells that survived, whether cut in regime I or II, had low levels of fluorescence. This result indicates that all cells that survived the cut must have also healed the membrane ruptures in 24 h.

Self-Cleaning of the Knife and Increasing Cutting Throughput. After cutting, we observed that cell residues were sometimes left at the knife tip (Fig. 4*A*). This observation was similar to that reported in previous studies on the splitting of droplets past an obstacle (e.g., a pillar) in a channel, where a small residual drop was left upstream of the obstacle under certain flow conditions (38, 39). The cell residue left behind was significantly smaller than the size of the cell (<10% of uncut cell size). This loss of cell mass did not seem to impair the healing and regeneration of the cell fragments. After about 5–10 cuts, however, the knife became blunted due to the accumulation of cell residues, which also started to clog the channels. The cutting of subsequent cells became difficult: Cells

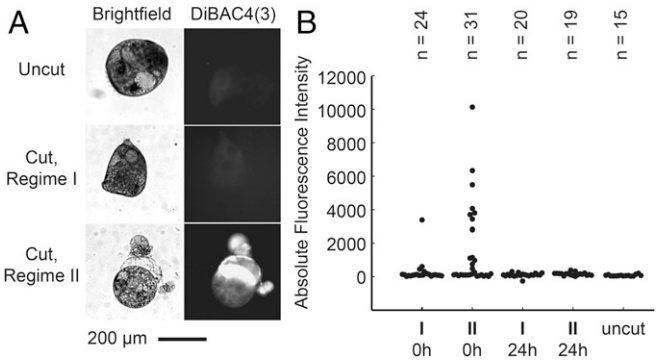

Fig. 3. Imaging the degree of membrane rupture. (*A*) Bright-field (*Left*) and DiBAC4(3) fluorescence (*Right*) images of uncut *Stentor* cell, a cell fragment cut in regime I, and a cell fragment cut in regime II, respectively. These cells were cut at the flow conditions indicated by blue arrows in Fig. 2 *B* and *C*. (*B*) DiBAC4(3) fluorescence intensities from cells cut in regime I and in regime II, where DiBAC4(3) was added immediate after the cut ("0h") or 24 h after the cut ("24h"). The fluorescence intensity of uncut cells is shown as a benchmark. Each marker represents the data for one cell.

would either squeeze through the clogged channel and lose much of their cytoplasm, become stuck at the knife, thereby clogging the channel further, or go down one outlet without being cut.

To generate a sufficient number of cells (>100) for studies such as RNA sequencing, a method to clean the knife was necessary. We found that the encapsulation of *Stentor* in aqueous drops before cutting facilitated the self-cleaning of the knife (*SI Materials and Methods* and Movie S6). Surface tension between the aqueous media and the oil facilitated the retaining of cell fragments within the drop, thereby preventing residues from accumulating on the knife (Fig. 4*B*). Fig. 4*A* shows that the knife was still clean after 10 cuts when cells were encapsulated in drops, whereas significant cell residues accumulated after 10 cuts when cells were not in drops. Significantly, we note that the ability to encapsulate and cut cells in droplets makes our method directly compatible with library preparation of cells within droplets for single-cell RNA sequencing and other droplet-based next-generation sequencing approaches.

In previous sections we identified a threshold velocity above which cell viability decreased rapidly at the transition of regime I and II. This threshold velocity sets the fastest rate for cutting a single cell, whether encapsulated inside a drop or not. At the concentration of cells used in our experiments we achieved a maximum cutting throughput of about eight cells per minute in a single microguillotine. To increase the throughput further, we designed a device consisting of eight parallel droplet generators each followed by a knife downstream (Fig. 4*C* and Fig. S4). Using this parallel device we achieved a cutting throughput of 64 cells per minute, >200 times faster than that when cutting cells by hand (Fig. 4*D*). Because the time scale for regeneration is about 10 h (13), this throughput is sufficient to generate enough cell fragments that are relatively synchronized in their stage of healing and regeneration for subsequent RNA sequencing experiments. The mean survival rate in cells cut by this parallel device was 94% (measured across three separate experiments), similar to the maximum survival rate for cells cut by a single knife.

Conclusions

We have reported a demonstration of a microfluidic guillotine device for the high-throughput cutting of *Stentor*. Examining the local cutting dynamics reveals two regimes under which cells are cut. In regime I, the low viscous stress causes the cell to wrap around the knife and cell splitting occurs at the cell's rear end, where the membrane pinches off at the knife tip. Wound size is well-controlled, and cell survival is close to 100%. In regime II, the high viscous stress causes the cell to deform extensively. The membrane often ruptures at random locations, generating multiple cell fragments with variable wound sizes. Cell viability decreases rapidly. The threshold velocity at which regime I transitions to II governs the maximum cutting throughput while maintaining high cell viability. Parallelizing the microguillotines increases the throughput to 64 cells per minute, two orders of magnitude faster than that by manual cutting. Our method is therefore capable of preparing hundreds of cells in a relatively synchronized stage of their wound repair, which is intrinsically a dynamic and time-dependent process. The identification of the two regimes of cutting with and without extensive membrane rupture provides opportunities to probe wound healing and regeneration separately. The ability to cut cells inside droplets further allows one to exploit existing droplet microfluidics techniques for next-generation sequencing analysis.

Real-time imaging of the membrane during the cut will allow for the identification of the position and the size of membrane ruptures. The measurement of the mechanical properties of *Stentor*, such as membrane tension, will further enable the prediction of cell response during the cutting process and will guide the design and the further development of the microguillotine for increased control of wounding.

The development of standardized tools and assays was critical for progress in the field of tissue-level wound healing, because they allowed different perturbations to be compared across samples with similar wound sizes in similar stages of the repair process. Our microfluidic platform presents an important step toward such a standardized assay and is expected to lay the foundation for understanding how single cells repair themselves. Furthermore, it should be possible to adapt our microguillotine design to other cell types. For cells of the size of a few microns or bigger, the soft lithographic method we had used to fabricate the microchannel and the knife can still be used. The material we had used was effective for cutting soft cells such as *Stentor*. For cells with increased stiffness, polymers (e.g., polycarbonate) with a higher elastic modulus than PDMS can be used.

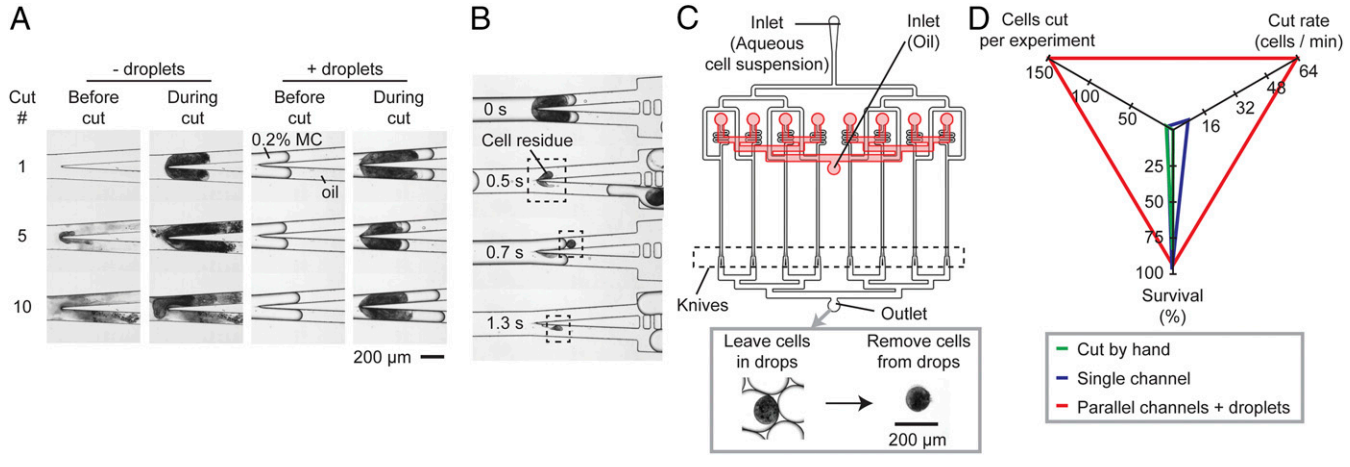

Fig. 4. Self-cleaning of the knife using droplets and parallelization of microfluidic guillotine device. (*A*) Micrographs of the knife after cutting 1, 5, and 10 cells, respectively, for the cases when the cells are not encapsulated inside droplets ("− droplets"), and when the cells are encapsulated inside droplets containing 0.2% wt/vol methylcellulose "MC" solution ("+ droplets"). (*B*) Micrographs showing the time sequence of the removal of cell residue by droplets. (*C*) Scheme showing the design of the parallel microfluidic guillotine device, containing eight parallel T-junction droplet generators where the cells are encapsulated into droplets and eight sets of knives downstream. (*C*, *Inset*) Micrographs showing the cut cell inside a droplet collected at the outlet of the device. The drops can be merged subsequently and the cell fragments can be collected and imaged out of the drops. (*D*) Comparison of the cutting performance using a glass needle by hand, a single microfluidic guillotine channel, and eight parallel channels where cells are also encapsulated in droplets.

Materials and Methods

Analysis of *Stentor* Morphology During Cutting. To characterize the cutting process in the microfluidic guillotine device we used a high-speed camera (Phantom v7.3) mounted on an inverted microscope with a 5× objective to record videos of the process.

To extract the extension length of the cells we used ImageJ. We defined the extension length to be the length of the cell fragment measured from the tip of the knife to the edge of the cell fragment that was the furthest away from the knife tip. We recorded the maximum extension length of each cell fragment in the frame immediately before the cut was complete, defined as the time when the two cell fragments detached from each other. The maximum extension length was then normalized to the length of the major axis of the uncut *Stentor* before it contacted the knife. In this paper, we report the normalized maximum extension length as ε_{max}. See *SI Materials and Methods* for more details.

Measurement of Cell Survival Rate After the Cut. To quantify the number of cells that survived the cut we collected the cell fragments from the device into a Petri dish containing pasteurized spring water (PSW). We monitored the morphology of the cells manually under a bright-field stereomicroscope. Because the membrane of *Stentor* disintegrates quickly after death, we classify a cell to be alive and to have regenerated successfully if (*i*) it has restored membrane integrity demonstrated by beating cilia and (*ii*) it is either actively swimming or attached to a surface in its namesake trumpet-like shape 24 h after the cut, a typical duration of time for *Stentor* to complete regeneration (8). A grid was drawn on the bottom of the Petri dish to facilitate counting of live cells.

To quantify the survival rate, we measured the number of live cells 24 h after the cut, $N_{post-cut}$. The survival rate is defined as $N_{post-cut}/2 \cdot N_{pre-cut}$, where $N_{pre-cut}$ is the number of cells injected into the device, counted manually from the videos of the cutting process. As a benchmark, we compared cuts using our device to cuts performed by hand, the conventional wounding method in previous regeneration studies (8). To cut cells by hand, we heated a glass capillary over a flame and stretched it into a thin needle (tip diameter ~30 μm), which was then cooled to room temperature before cutting through a cell that was immobilized in a 2% wt/vol methylcellulose solution. This solution was sufficiently viscous to reduce cell movement during cutting. After cutting, we added PSW to dilute the methylcellulose solution for subsequent monitoring of regeneration.

ACKNOWLEDGMENTS. We thank the Marine Biological Laboratory Physiology Course 2014 at Woods Hole, MA (supported by NIH Grant R13GM085967), for initial discussions and experimentations. This work was supported by NSF Grant MCB 1517089, National Institute of General Medical Sciences, NIH Grant T32GM008412 (to L.R.B.), NIH Grant GM113602 (to W.F.M.), American Cancer Society Fellowship 126787-PF-14-180-01-DMC (to P.S.), NSF CAREER Grant 1454542 (to S.K.Y.T.), and NSF Grant 1548297 (to L.R.B., J.W.K., W.F.M., and S.K.Y.T.). Parts of this work were performed at the Stanford Soft & Hybrid Materials Facility and the Stanford Nano Shared Facilities. The content of this work is solely the responsibility of the authors and does not necessarily represent the official views of the funding agencies.

1. Sonnemann KJ, Bement WM (2011) Wound repair: Toward understanding and integration of single-cell and multicellular wound responses. *Annu Rev Cell Dev Biol* 27:237–263.
2. Bement WM, Yu H-YE, Burkel BM, Vaughan EM, Clark AG (2007) Rehabilitation and the single cell. *Curr Opin Cell Biol* 19:95–100.
3. Tang SKY, Marshall WF (2017) Self-healing cells: How single cells heal membrane ruptures and restore lost structures. *Science* 356:1022–1025.
4. McNeil PL, Miyake K, Vogel SS (2003) The endomembrane requirement for cell surface repair. *Proc Natl Acad Sci USA* 100:4592–4597.
5. McNeil PL, Steinhardt RA (2003) Plasma membrane disruption: Repair, prevention, adaptation. *Annu Rev Cell Dev Biol* 19:697–731.
6. Zhao Y, Ishibashi S, Amaya E (2012) Reverse genetic studies using antisense morpholino oligonucleotides. *Methods Mol Biol* 917:143–154.
7. Slabodnick MM, Marshall WF (2014) Stentor coeruleus. *Curr Biol* 24:R783–R784.
8. Slabodnick MM, et al. (2014) The kinase regulator mob1 acts as a patterning protein for stentor morphogenesis. *PLoS Biol* 12:e1001861.
9. Slabodnick MM, et al. (2017) The macronuclear genome of Stentor coeruleus reveals tiny introns in a giant cell. *Curr Biol* 27:569–575.
10. Miyake A, Harumoto T, Iio H (2001) Defence function of pigment granules in *Stentor coeruleus*. *Eur J Protistol* 37:77–88.
11. Morgan TH (1900) Regeneration of proportionate structures in Stentor. *Biol Bull* 2: 311–328.
12. Lillie FE (1896) On the smallest parts of *Stentor* capable of regeneration: A contribution on the limits of divisibility of living matter. *J Morphol* 12:239–249.
13. Tartar V (1961) *The Biology of Stentor* (Pergamon, New York).
14. Fry HJ (1924) Cell dissection by hand. *Anat Rec* 28:371–377.
15. Chambers R (1918) The microvivisection method. *Biol Bull* 34:121–136.
16. Thalhammer S, et al. (2003) Laser microtools in cell biology and molecular medicine. *Laser Phys* 13:681–691.
17. König K, Riemann I, Fischer P, Halbhuber KJ (1999) Intracellular nanosurgery with near infrared femtosecond laser pulses. *Cell Mol Biol* 45:195–201.
18. Berns MW, et al. (1981) Laser microsurgery in cell and developmental biology. *Science* 213:505–513.
19. Magidson V, Loncarek J, Hergert P, Rieder CL, Khodjakov A (2007) Laser microsurgery in the GFP era: a cell biologist's perspective. *Methods Cell Biol* 82:239–266.
20. Shen Y, et al. (2011) Evaluation of nanoknife's edge angle for single cell cutting by using nanorobotic manipulators inside ESEM. *Proceedings of the 11th IEEE Conference on Nanotechnology* (IEEE, Piscataway, NJ), pp 155–160.
21. Alonso JL, Goldmann WH (2003) Feeling the forces: Atomic force microscopy in cell biology. *Life Sci* 72:2553–2560.
22. Agresti JJ, et al. (2010) Ultrahigh-throughput screening in drop-based microfluidics for directed evolution. *Proc Natl Acad Sci USA* 107:4004–4009.
23. Schmid L, Weitz DA, Franke T (2014) Sorting drops and cells with acoustics: Acoustic microfluidic fluorescence-activated cell sorter. *Lab Chip* 14:3710–3718.
24. de Terra N (1975) Evidence for cell surface control of macronuclear DNA synthesis in Stentor. *Nature* 258:300–303.
25. Moeendarbary E, et al. (2013) The cytoplasm of living cells behaves as a poroelastic material. *Nat Mater* 12:253–261.
26. Fletcher DA, Mullins RD (2010) Cell mechanics and the cytoskeleton. *Nature* 463: 485–492.
27. Takamatsu H, Rubinsky B (1999) Viability of deformed cells. *Cryobiology* 39:243–251.
28. Takamatsu H, Takeya R, Naito S, Sumimoto H (2005) On the mechanism of cell lysis by deformation. *J Biomech* 38:117–124.
29. Huang B, Pitelka DR (1973) The contractile process in the ciliate, Stentor coeruleus. I. The role of microtubules and filaments. *J Cell Biol* 57:704–728.
30. Wood DC (1970) Electrophysiological studies of the protozoan, Stentor coeruleus. *J Neurobiol* 1:363–377.
31. Jones AR, Jahn TL, Fonseca JR (1970) Contraction of protoplasm. 3. Cinematographic analysis of the contraction of some heterotrichs. *J Cell Physiol* 75:1–7.
32. Slabodnick M, Prevo B, Gross P, Sheung J, Marshall W (2013) Visualizing cytoplasmic flow during single-cell wound healing in Stentor coeruleus. *J Vis Exp* (82):e50848.
33. Tartar V (1953) Chimeras and nuclear transplantations in ciliates, *Stentor coeruleus* X *S. polymorphus*. *J Exp Zool* 124:63–103.
34. Tartar V (1956) Grafting experiments concerning primordium formation in *Stentor coeruleus*. *J Exp Zool* 131:75–121.
35. Adams DS, Levin M (2012) Measuring resting membrane potential using the fluorescent voltage reporters DiBAC4(3) and CC2-DMPE. *Cold Spring Harb Protoc* 2012:459–464.
36. Epps DE, Wolfe ML, Groppi V (1994) Characterization of the steady-state and dynamic fluorescence properties of the potential-sensitive dye bis-(1,3-dibutylbarbituric acid)trimethine oxonol (Dibac4(3)) in model systems and cells. *Chem Phys Lipids* 69:137–150.
37. Wood DC (1982) Membrane permeabilities determining resting, action and mechanoreceptor potentials in *Stentor coeruleus*. *J Comp Physiol* 146:537–550.
38. Chung C, Ahn KH, Lee SJ (2009) Numerical study on the dynamics of droplet passing through a cylinder obstruction in confined microchannel flow. *J Non-Newt Fluid Mech* 162:38–44.
39. Li Q, Chai Z, Shi B, Liang H (2014) Deformation and breakup of a liquid droplet past a solid circular cylinder: A lattice Boltzmann study. *Phys Rev E Stat Nonlin Soft Matter Phys* 90:043015.
40. Gorman DS, Levine RP (1965) Cytochrome f and plastocyanin: Their sequence in the photosynthetic electron transport chain of Chlamydomonas reinhardi. *Proc Natl Acad Sci USA* 54:1665–1669.
41. Son Y (2007) Determination of shear viscosity and shear rate from pressure drop and flow rate relationship in a rectangular channel. *Polymer (Guildf)* 48:632–637.
42. Garstecki P, Fuerstman MJ, Stone HA, Whitesides GM (2006) Formation of droplets and bubbles in a microfluidic T-junction-scaling and mechanism of break-up. *Lab Chip* 6:437–446.
43. Holtze C, et al. (2008) Biocompatible surfactants for water-in-fluorocarbon emulsions. *Lab Chip* 8:1632–1639.